Construction and Building Materials 337 (2022) 127511

Contents lists available at ScienceDirect

Construction and Building Materials

journal homepage: www.elsevier.com/locate/conbuildmat

Effects of spatial variability and correlation in stochastic discontinuum analysis of unreinforced masonry walls

Semih Gonen [a,*], Bora Pulatsu [b], Ece Erdogmus [c], Paulo B. Lourenço [d], Serdar Soyoz [e]

[a] Oslo Metropolitan University, Department of Civil Engineering and Energy Technology, Oslo, Norway
[b] Carleton University, Department of Civil and Environmental Engineering, Ottawa, ON, Canada
[c] Georgia Institute of Technology, School of Building Construction, Atlanta, GA, United States
[d] Institute of Sustainability and Innovation in Structural Engineering, University of Minho, Portugal
[e] Bogazici University, Department of Civil Engineering, Istanbul, Turkey

ARTICLE INFO

Keywords:
Stochastic analysis
Masonry
Uncertainty quantification
Spatial correlation
Monte Carlo simulation
Discontinuum analysis
Discrete Element method

ABSTRACT

This study investigates the influence of the uncertainty in material properties on the in-plane lateral behavior and capacity of stone masonry walls via a stochastic discontinuum analysis framework. The framework is demonstrated via the 3D numerical assessment of an unreinforced masonry (URM) wall using a stochastic analysis in the form of Monte Carlo simulations. The random parameters considered in this study are the prism compressive strength of masonry, the tensile strength of the masonry units and joints, and the friction angle for joints and units. Novel research is conducted using a fast and accurate DEM model to determine whether the spatial variability of the material properties should be taken into account. In addition, the effects of joint-to-joint correlation of modeling parameters are examined to identify if such a correlation exists. A total of 1200 stochastic discontinuum analyses for 12 different cases are carried out. The results call attention to considering the spatial variability of the modeling parameters in the stochastic analysis, as they significantly reduce the variation in the wall's strength and displacement capacity. Results also demonstrate the influence of the correlation between bed-joint parameters on the strength and failure mode of the walls. Ultimately, propagation of the uncertainty in the joint friction angle into the strength and displacement capacity of the walls is quantified.

1. Introduction

Unreinforced masonry (URM) structures constitute a remarkable portion of the existing building stock worldwide. As evidenced by past earthquakes, often, these structures are vulnerable to seismic actions due to their high mass and low tensile strength [1–3]. As a result, accurate prediction of their seismic behavior becomes essential to prevent severe structural failures and expensive repair costs. However, the composite and complex nature of masonry, inherent variability of its mechanical properties, and the unavailability of performance criteria for specific masonry typologies and failure mechanisms, are some of the factors that make this task challenging. To address inevitable uncertainty in the mechanical properties, probabilistic analysis of masonry structures has been studied in the last decades [4–10].

The capacity and behavior of URM walls, with respect to both in-plane and out-of-plane directions, are significantly influenced by the intrinsic features of masonry construction. For instance, the workmanship (*i.e.*, bond patterns, construction quality, etc.), aging, and past interventions have a considerable effect on the structural behavior of URM walls, as discussed in [11–14]. Similarly, the mortar type and its mechanical properties can noticeably influence joint behavior, hence, overall masonry strength [15,16]. In URM elements and systems, unit properties also inherently vary. While the variation in the units' properties is smaller in clay or concrete masonry manufactured through standardized methods, it is potentially a major variant in traditional hand-made brick or adobe, stone, and other forms of natural masonry. Nevertheless, these small and large variations in each of the components of masonry construction (both at the time of construction and throughout its lifetime) result in a structural system subject to high spatial variation in joint and unit parameters. This, in turn, alters the macro mechanical properties of the system, such as the overall force–displacement behavior and ultimate load resistance capacity. In this regard, important research questions for the seismic assessment of URM walls are, *i*) Should we consider the spatial variation of material and

* Corresponding author.
E-mail address: semihgon@oslomet.no (S. Gonen).

https://doi.org/10.1016/j.conbuildmat.2022.127511
Received 22 September 2021; Received in revised form 31 March 2022; Accepted 11 April 2022

joint properties in computational modeling of masonry walls? *ii*) If we consider spatial variation in properties, to what extent does it affect the results?

So far, few studies have addressed these questions partially, and none has systematically covered them using a stochastic DEM that forms the focus of this paper. Li et al. [17] used stochastic Finite Element (FE) analysis with 3D nonlinear elements to predict the strength of unreinforced masonry walls in vertical bending. They found considerable differences in results between the *spatial* and *non-spatial* analyses. Later, they extended their work [18] to URM walls under two-way bending. Comparison of the numerical and experimental results revealed that the spatial stochastic analysis captured the wall failure progression better. Müller et al. [19] investigated the effect of *spatial variability* of compressive strength and elasticity modulus on the reliability estimation of URM walls under compression. Recently, Gooch et al. [20] performed spatial and non-spatial stochastic FE analysis to estimate the variability of the capacity and failure modes of arched pier-spandrel systems subjected to in-plane shear loading. The FE micro-modeling technique is used in all these studies, which requires high computation demand. Alternatively, only a few studies used the discrete element method (DEM) and spatial/nonspatial stochastic discontinuum analysis (S-DA) to analyze load-bearing masonry systems and combined experimental and analytical investigations [21–23].

Another under-explored subject is the testing and simulations of spatial correlation of the strength parameters at the units and joints. Relatively minimal effort has been directed towards investigating unit-to-unit or joint-to-joint spatial correlation of properties and their impact on the wall strength and displacement capacity. Intuitively, one may assume a certain degree of correlation due to the construction process of masonry walls for example, use of the same batch of mortar or similar environmental deterioration in areas of proximity; however, it is not easy to quantify such correlations. To this end, this study also seeks answers to the following questions: *i*) If there exists a unit-to-unit or joint-to-joint correlation, how does it affect the overall force–deformation behavior of URM walls? *ii*) Does the unit-to-unit or joint-to-joint correlation significantly change the ultimate strength or damage progression? *iii*) Ultimately, should we consider any correlation in spatial stochastic modeling?

In the pioneering work of Heffler et al. [24], the authors assessed the spatial correlation of unit flexural bond strengths within and between the courses, using six full-sized clay brick URM walls and bond-wrench testing on masonry units. They concluded that the flexural bond strengths of joints are statistically independent. However, their research was limited to the particular type of material, size and aspect ratio of the units, and the specific geometry of masonry walls. Outside of Heffler's study, experimental studies investigating the questions posed are scarce because a statistically significant experimental study on the variability of properties requires infeasibly large sample sizes. In this context, advanced numerical models can provide the necessary means to overcome the limitations posed by experiments, as they enable the simulation of various configurations. Still, very few studies of this nature exist: Li et al. [25] conducted stochastic 3D FE analyses to examine how correlation and spatial variability of modeling parameters affect the strength and damage of clay brick URM beams. Tabbakhha and Deodatis [26] analyzed the behavior of URM walls for the different spatially correlated tensile strengths of mortar joints as the only random parameter considered in that study. Their results showed that the close correlation of bed joint properties along a course of the wall reduced the lateral strength of the investigated wall. Isfeld et al. [27] carried out a stochastic assessment of clay brick URM walls in one-way bending to study the effect of wall length on the ultimate load. It was observed that the analysis results converged to the experimental ones the most when the spatial correlation of parameters was included.

Another critical aspect of stochastic modeling of URM walls is uncertainty propagation, *i.e.*, how the outcome reflects the uncertainty associated with the input. Existing studies in masonry buildings [4,28,29] mostly incorporate simplified and homogeneous approaches using the Finite Element Method; however, there is scarcity in terms of the more advanced micro-modeling approach and the impact of the modeling parameters. As shown in earlier studies of stochastic micro-modeling of masonry walls [6,21,22,30], masonry strength is highly correlated with the friction angle value of its joints (especially for dry-joint and low-bond strength URM masonry walls). However, the probability distribution and its parameters for the random variables are often not available. Therefore, several assumptions must be made, such as the coefficient of variation of friction angle, and their effects on the results mostly remain unnoticed. In this context, this study investigates how the variations in joint friction angle affect the force–displacement behavior and in-plane strength of the URM walls through stochastic discontinuum analysis (S-DA) based on the DEM.

It can be seen that there is enough evidence from prior experimental and numerical studies that hint at the fact that a more systematic approach to stochastic analysis can lead to more accurate predictions of the seismic behavior of URM walls; however, further research is needed to quantify these benefits with respect to the cost of performing more complex analyses.

This study examines several research questions raised above using stochastic discontinuum analyses and contributes to the state-of-the-art stochastic discontinuum analysis of masonry structures. The proposed DEM-based modeling approach offers a more accurate representation of URM walls by comparing a large set of stochastic numerical analyses with a previously published experimental data set. The modeling approach considers all possible damage scenarios observed in the experiments, including sliding failure, tensile cracking, and crushing. A total of 1200 S-DA are performed, considering the spatial variation of the joint properties as statistically uncorrelated variables ($\rho = 0$) as well as correlated with different factors ($\rho = 0.65$, $\rho = 0.85$ and $\rho = 1.00$). Note that when the spatial correlation ρ goes to unity, it represents the case where the mechanical properties are uniform along the entire wall. Furthermore, the direct influence of the coefficient of variation (CoV) of the joint friction angle on the results is studied by considering three different values of CoV (0.25, 0.15, and 0.05).

The paper is organized as follows: In Section 2, the mathematical background of the employed modeling strategy and the proposed stochastic analysis framework are explained. In Section 3, the spatial and non-spatial analysis results are presented and compared. Then, in Section 4, the influence of the CoV of the joint friction angle on the behavior and capacity of the URM wall is evaluated. Furthermore, the propagation of the uncertainty in the input parameters into the results is quantified. In Section 5, the joint-to-joint spatial correlation of modeling parameters is investigated, and finally, conclusions are derived in Section 6.

2. Stochastic discontinuum modeling

The inherent variation in the masonry properties and uneven deterioration of masonry across its different areas results in an overall uncertainty in the mechanical properties of walls. Even in a controlled laboratory environment, noticeable variations in the results can be observed due to the heterogeneous characteristics of the masonry. For simplicity, masonry structures are often analyzed using deterministic models; hence, the probabilistic nature of their mechanical properties is ignored. On the other hand, stochastic models provide more realistic solutions for the structural engineering problems associated with random variables, such as material properties, loads, and boundary conditions [31]. Several recent examples regarding the probabilistic seismic assessment of masonry structures have demonstrated the importance of stochastic modeling and the need for substantial research to quantify the uncertainties in the analysis, both at component and system levels [32–34].

In this study, a DEM-based stochastic discontinuum analysis framework is proposed to assess a URM masonry wall subjected to lateral

loading. First, the employed modeling approach is validated against a benchmark study, a recent experimental work where a URM stone masonry wall is tested under combined compression and in-plane shear loadings. After the capacity and behavior predictions of the wall are demonstrated to match the experimental results, uncertain model parameters are introduced, and the stochastic analysis is conducted.

Please note that this study considers only the parameter uncertainty stemming from imprecise model input values. Other types of uncertainties such as numerical uncertainty, bias error due to our idealizations of the boundary conditions and acting forces, and experimental uncertainty are not taken into account.

2.1. Background on the numerical DEM procedure

The computational modeling of masonry structures has been an active research field for the last several decades. Different numerical techniques and strategies have been proposed by researchers considering various levels of complexities, relying on continuum and discontinuum-based computational formulations [35–40]. In this research, the latter approach is utilized to analyze a URM wall based on the discrete element method developed by Cundall [41]. The proposed DEM-based model can be categorized as a simplified micro modeling approach, where the units are expanded to include half-mortar thickness, similarly to previous studies [30,42,43].

In DEM, the load-bearing masonry systems are replicated via individual rigid or deformable blocks with zero-thickness interfaces, in which the blocks can interact with each other along their boundaries. Deformability is introduced by discretizing the blocks into tetrahedral zones (volumes in 3D), which may undergo elastic or plastic deformations. However, it is worth noting that the choice of a rigid or deformable block in DEM simulations is determined considering multiple factors, such as the physics of the problem, the research question sought, and the computational cost. For instance, rigid blocks are preferable in dynamic analysis since they require less computational time than deformable blocks, as Lemos [39] highlighted. On the other hand, deformable blocks can provide valuable information (if needed) regarding the elastic and plastic stress/strain histories developing within blocks, which may be necessary for specific problems (e.g., [44,45]). This research uses rigid blocks to simulate the URM wall behavior (different from the authors' recent work in which the deformable blocks were utilized for the same structure [21]). The primary motivation to utilize rigid blocks is to diminish the computational cost and run more analyses within a reasonable time. It takes approximately 9 min to analyze the benchmark study for the rigid block model for this specific problem, five times faster than the deformable block model using a computer system Intel® Core™ i7 CPU @ 2.7 GHz processor and 16 GB memory RAM. Note that the proposed modeling strategy offers less computational demand than the FEM-based micro-modeling approach, mentioned in other studies [25], even though they are not precisely comparable since different computer systems and structures are employed.

Briefly, the core idea of DEM relies on the explicit integration of equations of motions (both translation and rotational) for each block's center of mass. The new translational ($\dot{\boldsymbol{u}}^{t+}$) and rotational ($\boldsymbol{\omega}^{t+}$) velocities, which are evaluated at the mid-intervals of a time step, Δt (e.g., $t^+ = t + \Delta t/2$, $t^- = t - \Delta t/2$) are obtained as given in Equations (1) and (2), respectively.

$$\dot{\boldsymbol{u}}^{t+} = \dot{\boldsymbol{u}}^{t-} + \frac{\Delta t}{m}\boldsymbol{F}^{t} \tag{1}$$

$$\boldsymbol{\omega}^{t+} = \boldsymbol{\omega}^{t-} + \frac{\Delta t}{I}\boldsymbol{M}^{t} \tag{2}$$

where $\boldsymbol{F}$, $\boldsymbol{M}$, I, and m are the force vector, including the sum of contact forces and applied forces, the moment vector, consisting of moments developed by contact forces and applied forces, the mass moments of inertia, and block mass, respectively. Cundall's local damping formulation is utilized to obtain steady-state solutions (either corresponding to equilibrium or steady-state failure, *i.e.*, collapse) from the given dynamic equations, as discussed in the [46]. Moreover, the numerical stability is ensured using small time steps ($\Delta t < \Delta t_{critical}$). After the new velocities are calculated, the displacement ($\Delta \boldsymbol{x}$) and rotation ($\Delta \boldsymbol{\theta}$) increments are obtained using Equation 3 to get the new position of the block centroid ($\boldsymbol{x}^{t+}$), as written in Equation (4). Accordingly, block vertices and edge orientations are determined in order to compute contact (interaction) forces.

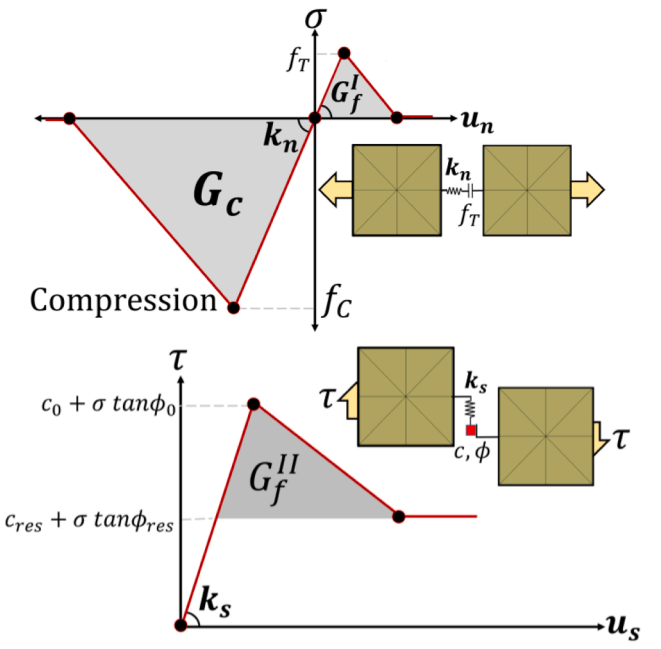

Fig. 1. Contact constitutive law defined at the contact point in the normal and shear directions: Tension-compression (Top); Shear (Bottom).

$$\Delta \boldsymbol{u} = \left(\dot{\boldsymbol{u}}^{t+}\right)\Delta t \tag{3a}$$

$$\Delta \boldsymbol{\theta} = \left(\boldsymbol{\omega}^{t+}\right)\Delta t \tag{3b}$$

$$\boldsymbol{x}^{t+} = \boldsymbol{x}^{t} + \Delta \boldsymbol{u} \tag{4}$$

Contact forces are computed based on the updated spatial configuration of the discontinuous system among the adjacent blocks. At each contact surface (also referred to as joint), orthogonal linear/nonlinear springs are defined for the prescribed contact points that control the contact stiffness and strength in normal and shear directions along the joint. Through this study, fracture energy-based contact constitutive models are utilized to better represent the post-peak response of the material [47,48]. As shown in Fig. 1, the Coulomb-Slip joint model is utilized with tension–compression elastic-softening behavior. The employed point contact approach requires normal (k_n) and shear (k_s) stiffness as well as initial and residual strength parameters. The tension–compression behavior is defined considering simple linear softening laws, requiring tensile strength (f_T), mode-I fracture energy (G_f^I) and compressive strength (f_C) with associated fracture energy (G_C), respectively. Moreover, the shear failure criterion is defined using cohesion (c_0), friction angle (ϕ_0), mode-II fracture energy (G_f^{II}), residual cohesion (c_{res}) and residual friction angle (ϕ_{res}), presented in Fig. 1. The damage in tension and shear is coupled using a single damage parameter, further explained in Pulatsu et al. [22].

It is important to note that the contact stiffnesses are only defined for the potential crack surfaces within the units (denoted as $k_{n,u}$ and $k_{s,u}$) and the unit-mortar interfaces ($k_{n,j}$, $k_{s,j}$), based on the horizontal (s_H) and vertical (s_V) joint spacings using Equation 5, in which k_j is estimated as

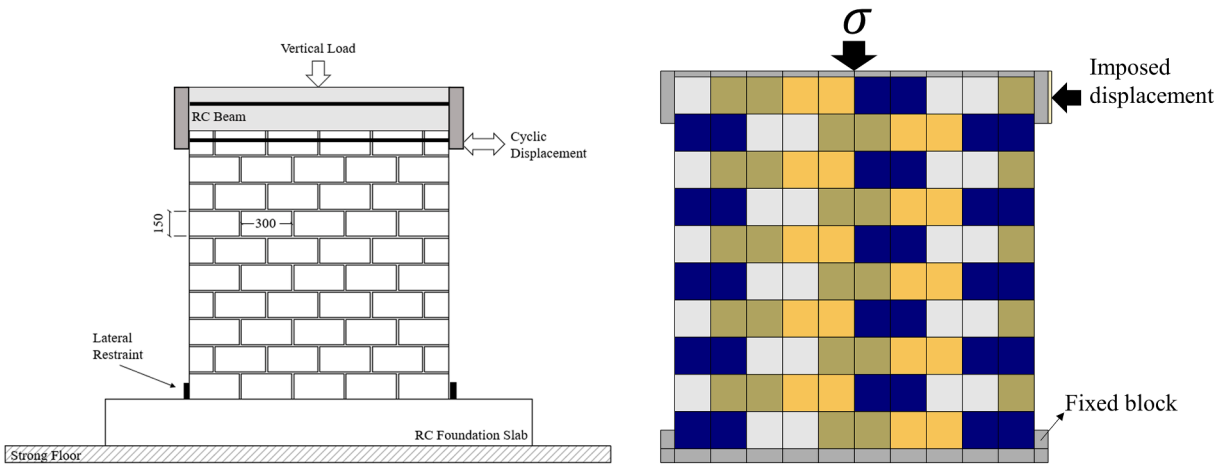

Fig. 2. Left: Illustration of the test setup; **Right**: Discrete Element model.

0.4 times k_n (see Equation 5) [49–51].

$$k_{n,u} = E_{unit}/s_H \& k_{s,u} = 0.4k_{n,u} \tag{5a}$$

$$k_{n,j} = E_{wall}/s_V \& k_{s,j} = 0.4k_{n,j} \tag{5b}$$

where E_{unit} and E_{wall} are Young's modulus for stone units and masonry walls.

The point contact stresses are obtained incrementally for normal ($\Delta\sigma$) and shear ($\Delta\tau$) directions. The executed contact stress computation relies on the predictor–corrector scheme, typically performed in a nonlinear explicit numerical solution. Initially, the elastic contact stress increments are obtained using Equation (6), where the relative point contact displacement is decomposed into the normal (Δu_n), and shear direction (Δu_s). Then, the obtained stress increment is added to the previous one to obtain the new contact stresses (see Equation (7)). If the new contact stresses violate the defined failure criteria, the new contact stresses are updated with the corrected one and multiplied with the associated contact area to be utilized as forces in equations of motion (as given earlier in Equations 1–2) [52].

$$\Delta\sigma = k_n \Delta u_n$$

$$\Delta\tau = k_s \Delta u_s \tag{6}$$

$$\sigma^{t+} = \sigma^t + \Delta\sigma$$

$$\tau^{t+} = \tau^t + \Delta\tau \tag{7}$$

The proposed DEM-based modeling framework is performed using a commercial three-dimensional discrete element code (3DEC) developed by ITASCA [53]. The proposed contact models are written in C++ and compiled as DLL (dynamic link library) into 3DEC via the user-defined constitutive model option. In the next section, validation of the proposed modeling strategy is presented.

2.2. Validation study

A laboratory experiment conducted by the authors was used to validate the proposed DEM procedure. A stone masonry wall with dimensions of 1.55 m × 1.60 m × 0.30 m was tested in reversed cyclic in-plane shear compression, and its constituents were characterized via several destructive and non-destructive tests. These laboratory tests have been extensively documented elsewhere [15,16,21], and they are not the focus of this study. However, all the necessary information to model the wall is presented herein.

The wall panel was constructed using ashlar stones and a commercial brand natural hydraulic lime (NHL) mortar. The wall base consisted of a

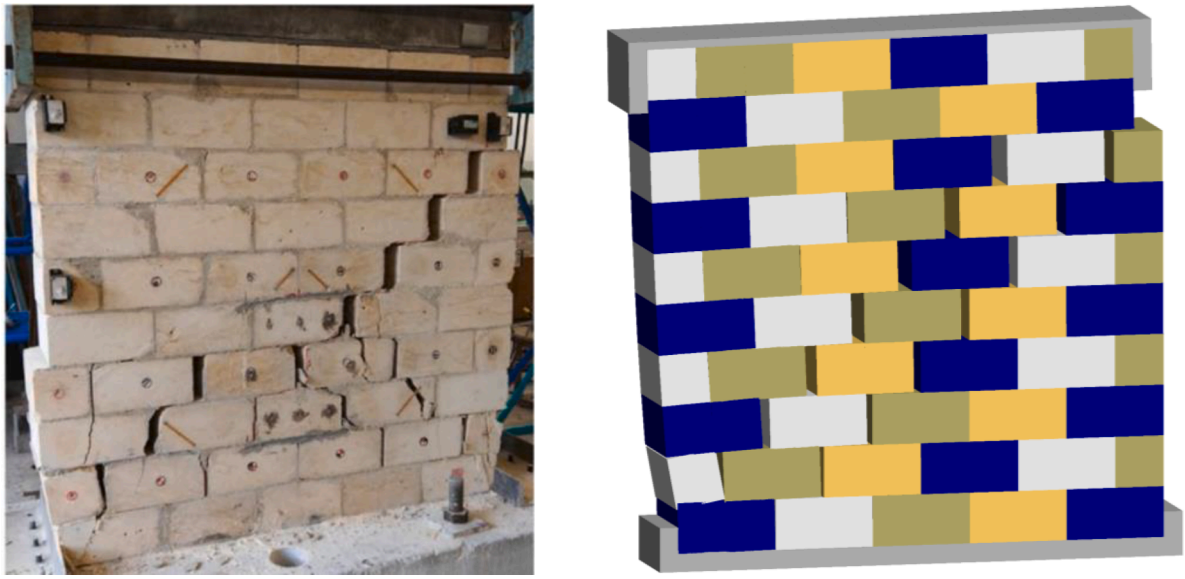

Fig. 3. Left: Stone masonry wall panel after the test; **Right**: Damage state of the wall at the last stage of the DEM analysis.

Table 1
Contact properties defined for unit-unit and unit-mortar interface interactions using in discrete element model to simulate the benchmark study.

Interaction within the stone masonry units			
$f_{t,u}$ (MPa)	c (MPa)	ϕ_u (°)	ϕ_{res} (°)
1	2	40	40
$f_{c,u}(MPa)$	$G_f^I(N/m)$	$G_f^{II}(N/m)$	$G_c(N/m)$
23.3	30	550	23000
Interaction between the masonry units			
$f_{t,j}(MPa)$	$c(MPa)$	$\phi_j(^\circ)$	$\phi_{res}(^\circ)$
0.2	0.2	30	30
$f_m(MPa)$	$G_f^I(N/m)$	$G_f^{II}(N/m)$	$G_c(N/m)$
5.5	5.8	0	8820

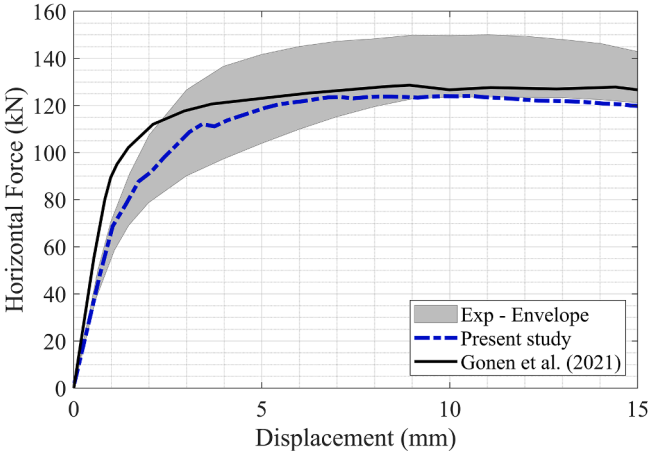

Fig. 4. DEM prediction from the deterministic DEM-based models vs. the experimental envelope curves.

reinforced concrete (RC) foundation and a cement-based high-strength mortar, connecting the structure to the RC foundation. At the base level, two C-shaped steel profiles at both sides of the wall prevented any lateral translation. The same high-strength mortar was also used at the top of the wall to bond the top layer of stones and prevent individual sliding of units. An RC loading beam at the top of the wall distributed the vertical load evenly, which caused mean compressive stress of 0.5 MPa. A rig was used to apply displacement-controlled lateral loading, clamped to the top layer of the stones and the RC spreader beam. Two roller supports on both sides of the walls prevented the out-of-plane movement of the walls. An illustration of the test setup is presented in Fig. 2.

During testing, the wall displayed a flexural rocking behavior at the beginning, causing cracks along the lower course of bed joints. Then, a mixed-type behavior was observed as a diagonal stepped-crack appeared through the stone-mortar interfaces. In the last cycles of testing, a bed-joint sliding combined with toe crushing was noted. Fig. 3 illustrates the final damaged state of the tested URM wall.

For the validation, boundary conditions and geometrical features of the URM wall are represented in the discrete element model. The lateral loading is imposed as a constant displacement rate of 5 mm/s. The mechanical properties used in the DEM model are taken from the available material characterization testing performed in the experimental study and presented in Table 1. Moreover, the necessary input of fracture energies is assumed based on the ductility index for tension, shear, and compression recommended in the literature [54]. The joint tensile strength ($f_{t,j}$) is approximately assumed as 5% of the masonry compressive strength (f_m). Note that the experimental material characterization was limited to the masonry compressive strength, and tensile and compressive strength of the units [16]. For the remaining properties, the same values utilized in a previous DEM-based study of this

Table 2
Variables, their associated distributions, and statistical parameters.

Random Variable	Probability Distribution	Mean (μ)	Coefficient of Variation (CoV)
f_m (MPa)	Normal	5.50	0.15
$f_{t,bond}$ (MPa)	Lognormal	0.25	0.45
$f_{t,unit}$ (MPa)	Lognormal	1.00	0.16
ϕ_{bond} (degrees)	Normal	35	0.25
ϕ_{unit} (degrees)	Normal	38	0.10
Dependent Variable	**Relationship**		
c_{unit} (MPa)	$2.0 f_{t,unit}$		
c_{bond} (MPa)	$1.0 f_{t,bond}$		
G_f^I (N/mm)	$0.029\ f_{t,bond}$		
G_C (N/mm)	$1.6\ f_m$		

structure [21] are adopted to be able to directly compare the results. All the values of the contact parameters used in the benchmark study are presented together in Table 1.

A similar damage progression to the experimental results is observed during the numerical analysis, consisting of flexural cracks and sliding failures at the bed joints, diagonal stair-step cracks, and compression failure at the toe of the wall, as shown in Fig. 3. Qualitative verification is established since the DEM model accurately simulates the damage progression and crack pattern. Quantitative agreement between the numerical and experimental results is also established, as shown in Fig. 4. The base shear force versus the lateral deflection at the top of the URM wall is compared against the experimental envelope and a previous DEM-based solution (made up of deformable blocks, [21]). In Fig. 4, the gray-shaded part represents the area between the positive envelope and the absolute value of the negative envelope curve (the reverse direction). For small displacements (less than 5 mm), the present model behavior falls right into the middle of the experimental positive and negative envelope curves (presented in absolute values) obtained from the cyclic-shear test. On the other hand, when the displacement is higher than 5 mm, the results converge to the lower bound of the experimental envelope. It is also worth noting that very close results are obtained from different DEM-based simulations, confirming that both approaches are acceptable. Considering the qualitative and quantitative match between the numerical and experimental results, the deterministic DEM model is validated.

2.3. Uncertainty in the model parameters

In the probabilistic analysis approach, the unit and joint properties are considered either deterministic, random, or dependent variables. This research focuses on the nonlinear parameters utilized in DEM; hence, the contact stiffness is kept constant in all analyses. The readers are referred to the earlier work of the authors discussing the influence of contact stiffness [22]. The parameters to which the strength and displacement capacity are the most sensitive are determined as random variables and presented in Table 2. They are the compressive strength of masonry (f_c), the bond (unit-mortar interface) tensile strength ($f_{t,bond}$), the tensile strength of units ($f_{t,unit}$), the friction angle within the units (ϕ_{unit}), and the friction angle for joints (ϕ_{bond}). Note that the cohesion of the unit and bond cohesion are considered as dependent variables with the relationships $c_{unit} = 2f_{t,unit}$ and $c_{bond} = f_{t,bond}$, respectively. Similarly, the fracture energies are calculated according to the corresponding strength values, considering the suggestions presented in the literature [54] and the expressions given in Table 2.

A normal distribution is assumed for the compressive strength of masonry, whereas the tensile strength of the units and bonds follow a lognormal distribution to prevent negative values during sampling, following the pertinent literature [21,25,32]. The statistical parameters of the compressive strength of masonry and the tensile strength of units

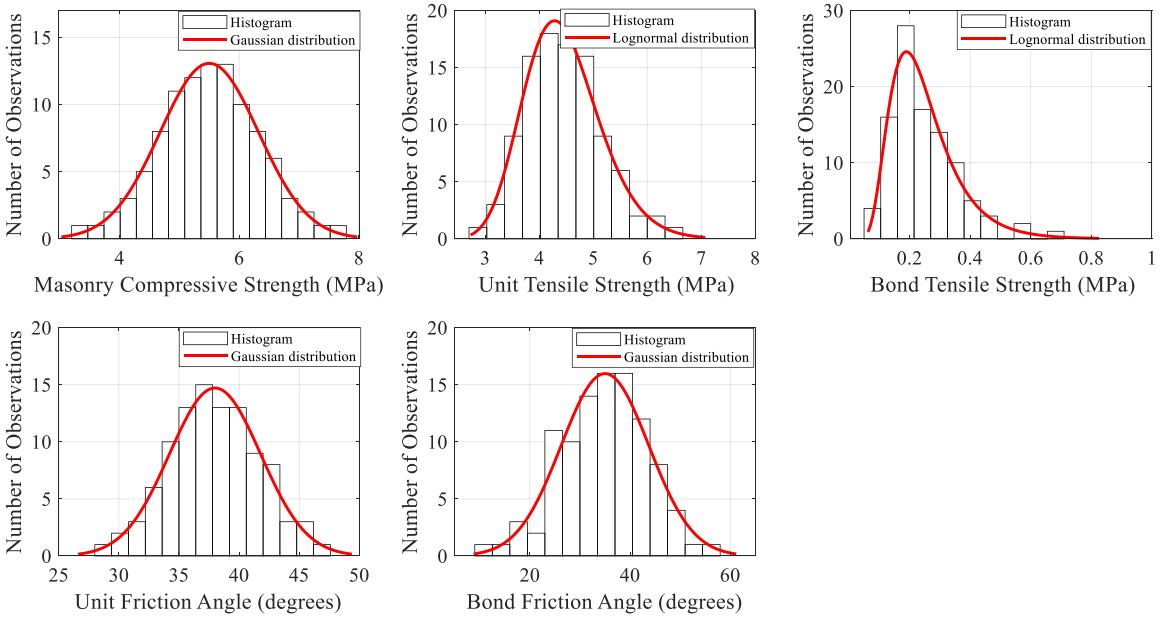

Fig. 5. Histograms and probability distributions of the sampled random variables for the benchmark case ($\rho = 1$ and $CoV_{\phi_{bond}} = 0.25$).

are obtained experimentally [16]. Also, a slightly higher coefficient of variation is assigned for the bond tensile strength due to highly scattered test results. It should be noted that the mean values of some parameters, taken as the deterministic values used in Table 1, are amended in Table 2. According to the previous studies, the joint and unit friction angle values and their CoV are revised [21,22].

The statistical parameters in Table 2 are used to define the prescribed distributions used in the Monte Carlo simulations (MCS). The Latin Hypercube Sampling (LHS) [55] method is used to reduce the variance in the derived samples. Indeed, the LHS technique has been used to improve the efficiency of sampling methods, resulting in significant savings on computational cost [56]. No correlation is specified between the parameters, *i.e.*, the random variables are statistically independent. Twelve different cases considered the changes in the spatial variation of the modeling parameters and the coefficient of variation of the joint (or bond) friction angle. In these cases, the spatial variation of the joint properties is either considered as statistically uncorrelated, I) $\rho = 0$, or correlated at different levels: II) $\rho = 0.65$, III) $\rho = 0.85$ and IV) $\rho = 1.00$. These four cases of spatial correlation are reiterated for the three values of the coefficient of variation of the joint friction angle: 0.25, 0.15, and 0.05. For instance, the four cases of spatial correlation are considered when CoV of the friction angle is 0.25, another four cases for CoV = 0.15 and the last four cases for CoV = 0.05. Thus, the total number of the cases adds up to 12. For each of the twelve cases, 100 simulations are run, *i.e.*, 100 values of each random variable are generated, from the corresponding probability distributions with a given mean and coefficient of variation. The total number of the simulations performed corresponds to1200.

Among these cases, the one that includes the non-spatial stochastic analysis with the coefficient of variation of the friction angle equal to 0.25 will be referred to as the "benchmark study" hereafter. As an example of the LHS sampling, the benchmark study is used to illustrate the independent random variables, their probability distributions, and the histograms of the sampled values, as shown in Fig. 5. Note that the sample size of the benchmark study is 100, as well as all for the other cases.

3. Spatial versus Non-Spatial S-DA

The mechanical properties of masonry components vary spatially due to several factors, such as the inherent variability of the material

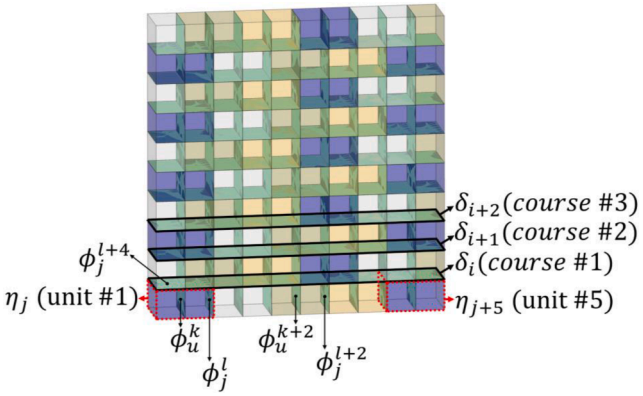

a) Contact surface numbering for unit and joints, $k \in [1..45]$; $l \in [1..135]$.

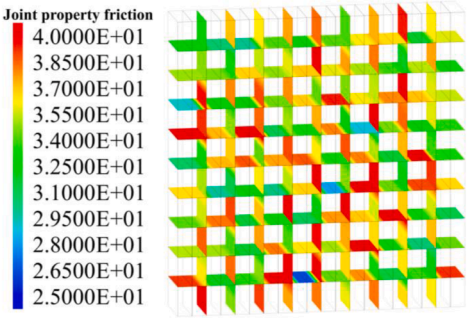

b) An example case for the spatial variation of friction angle ($25 \leq \phi \leq 40$)

Fig. 6. Numbering the contact surface and spatial variation of the contact friction angle.

properties, workmanship, and the uneven degradation of materials and joints. Aging mortar may soften and lose stiffness, and bond strength typically decreases over time as some of the mortar is lost. Interventions on existing structures are another source of variability: it is common to tuck parts of a wall with a different, typically stronger mortar, resulting in significantly different mortar properties across a wall's length/area. The spatial stochastic simulation is set up in the following way to address these phenomena: first, an identification number is defined for each joint (or contact plane) in the discrete block system, as illustrated in

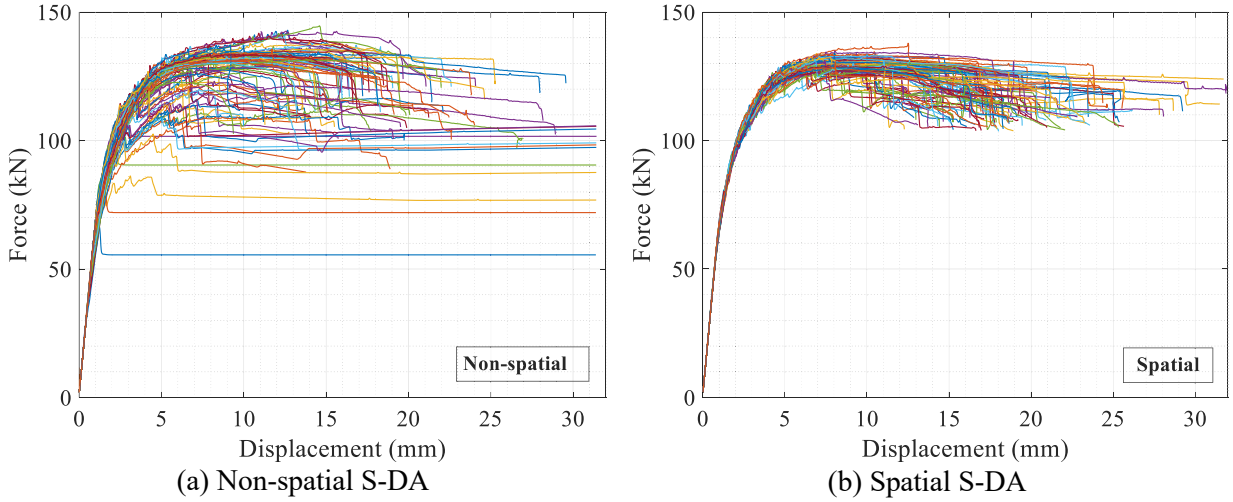

Fig. 7. Force-displacement curves obtained from the non-spatial and spatial S-DA.

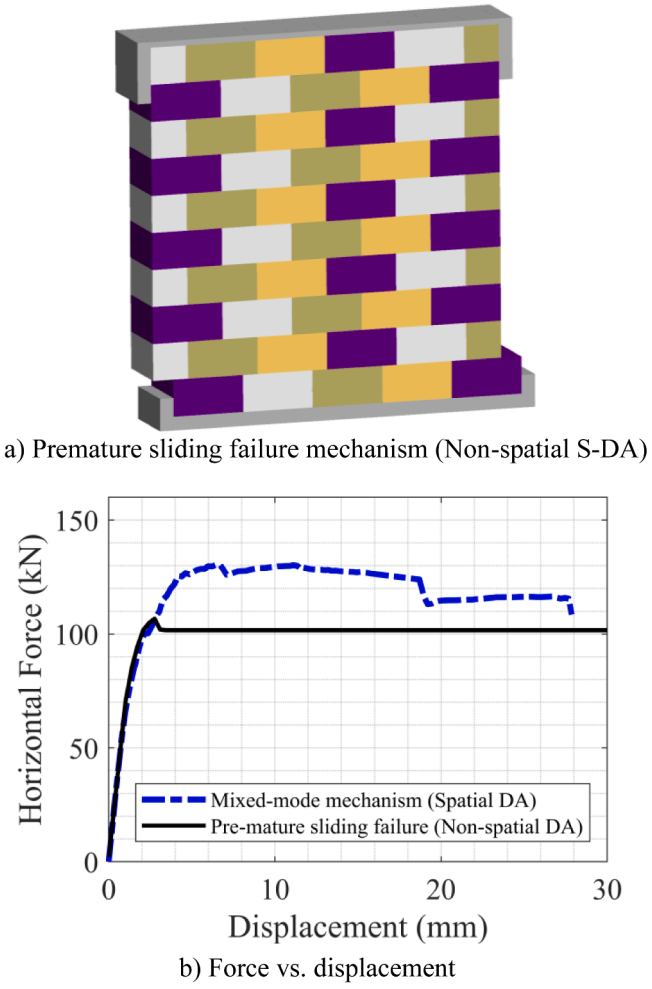

Fig. 8. Sliding failure (a) an example case, (b) force–displacement curve.

Fig. 6a. To effectively assign the mechanical properties of block units and bonds (or unit-mortar-interfaces), the joints within and in-between the units are grouped and numbered separately. There are 45 joints within units and 135 joints in-between them. Then, from the prescribed distributions given in Table 2, 135 different values of tensile strength, frictional resistance, and compressive strength are sampled using the LHS method and assigned to each joint in-between the units (see Fig. 6b). Similarly, each of the 45 joints within the units is assigned a different tensile strength and friction angle. Therefore, in a single simulation, 45 different values are sampled from the specified distribution for stone units, while 135 samples are generated for each parameter related to the masonry bond and compressive strength. The sampling process is repeated for each of the 100 simulations.

In a non-spatial stochastic analysis, the same probabilistic modeling strategy is used as the spatial analysis. However, this time, in each realization of the 100 Monte Carlo simulations, one value is generated for each modeling parameter given in Table 2. That value is assigned to all joints within or in-between the units, which results in a homogeneous distribution of material properties. Hence, two cases are simulated in this section: *i*) every unit and joint had the same value for each Monte Carlo simulation, *i.e.*, they did not differ spatially (referred to as non-spatial), and *ii*) joint properties spatially varied for each simulation.

The force–displacement curves obtained from non-spatial and spatial stochastic analyses are presented in Fig. 7. In this study, the ultimate lateral displacement is adopted as the point on the load–displacement curve where the ultimate load drops to 80% of the maximum load, if applicable. Otherwise, the analyses are run until 32 mm of displacement is reached (*i.e.,* final displacement corresponding to 2% drift ratio). However, it is noted that low friction angles yield approximately bilinear curves (Fig. 7a) associated with the bed-joint sliding. This type of behavior may be considered as premature failure, where the sliding mechanism is formed at an early stage along a large portion of a row of the wall, shown in Fig. 8a. The load is sustained with increasing displacements until the end of the analysis (see Fig. 8b). Twelve cases of such failure are observed in 100 simulations when using the non-spatial S-DA approach. In contrast, no premature sliding failure is observed in spatial S-DA, which can be noticed in Fig. 7b. Also, the graphs present a more uniform batch compared to non-spatial S-DA, signaling less variation in the maximum force and displacement values. The mechanics of spatial S-DA are different and more realistic than the nonspatial analysis since load redistributions become more influential due to the spatial variation of the material properties, revealing that sliding failures are less likely to occur. Note that the spatial variation of the joint properties is considered as statistically uncorrelated ($\rho = 0$). As demonstrated in the following sections, the amount of the statistical correlation might alter the results. The differences are further elaborated in the next section.

The bed joint sliding failure requires further discussion as it is also encountered in the rest of the present study. It occurs when the joint

Table 3
Average maximum force and displacement obtained from spatial and non-spatial S-DA.

		Non-spatial ($\rho = 1$) $CoV_{\phi_{bond}}$			Spatial ($\rho = 0$) $CoV_{\phi_{bond}}$		
		0.25	**0.15**	**0.05**	**0.25**	**0.15**	**0.05**
F_{max} (kN)	Mean	127.48	130.07	131.85	131.10	131.31	132.87
	CoV	0.101	0.061	0.031	0.015	0.015	0.019
D_{max} (mm)	Mean	19.10	18.83	18.04	19.45	18.82	19.07
	CoV	0.339	0.286	0.272	0.226	0.223	0.180
# of sliding failure		12	4	4	0	0	0

friction angle and tensile strength are low and compressive strength is higher. For the twelve cases encountered in the non-spatial S-DA, the mean values of the joint friction angle, joint tensile strength, and the compressive strength of masonry are 21.7 degrees, 0.21 MPa, and 5.75 MPa, respectively. As stated, Fig. 8a illustrates an example in which sliding along the bed joints dominates the behavior. The nonlinearity in the behavior starts with an initial horizontal crack, starting from the lower-right of the wall and reaching towards the left. As the units at the bottom-left corner of the wall do not fail in compression, a sliding mechanism develops, and the upper portion of the wall continues sliding above the lower part. Although this specific case is observed in several analyses, it may be a numerical artifact. In other words, this type of failure seems less likely in physical testing, according to the experience of the authors. In any case, one should be cautious about the large displacement capacity indicated by this failure mode.

4. Influence of the variation in joint friction angle

The impact of the joint friction angle on the force–displacement behavior has been demonstrated in the previous section. In this section, additional stochastic analyses are carried out to investigate it further and quantify its effect. The same procedure, as described in Section 3, is followed for sampling. The identical strength parameters and values (given in Table 2) are utilized in the analyses, except the coefficient of variation of the joint friction angle, assigned a value of 0.15 and 0.05 in two additional cases (*i.e.*, CoVs used are 0.05, 0.15, and 0.25). These two additional cases were carried out for non-spatial and spatial S-DA, resulting in 400 additional simulations. Therefore, six cases of non-spatial and spatial S-DA have been conducted. The outcomes are summarized in Table 3 in terms of the average maximum forces and displacements obtained.

The impact of the decrease in the coefficient of variation of the bond friction angle is remarkable for the non-spatial cases as it significantly reduces the variation in the maximum force and displacement. Almost a linear trend is observed: 40% decrease in the $CoV_{\phi_{bond}}$ (from 0.25 to 0.15) resulted in a 40% decrease in the $CoV_{F_{max}}$ (from 0.10 to 0.06); 80% decrease in the $CoV_{\phi_{bond}}$ (from 0.25 to 0.05) resulted in a 70% decrease in the $CoV_{F_{max}}$ (from 0.10 to 0.03). However, the change in the ultimate displacements is not significant, in contrast to the effect on maximum forces. This outcome is expected as the post-peak behavior of the stone masonry walls is typically dominated by several other factors than the joint friction angle. As opposed to the non-spatial S-DA, the decrease in the $CoV_{\phi_{bond}}$ causes no noticeable change in the spatial S-DA. It means that even if higher values of $\mathrm{CoV}_{\phi_{\mathrm{bond}}}$ are assumed for the bond friction angle, this will not alter the results substantially, demonstrating an appealing feature of spatial S-DA, especially when there is a lack of data (or experimental results) for input material properties.

In addition to the decrease in the number of sliding failures mentioned earlier, it is possible to notice other differences when the spatial and non-spatial results are compared. For the benchmark study (*i.e.*, non-spatial & $CoV_{\phi_{bond}} = 0.25$), the differences in the variation of the maximum forces and displacements are noteworthy when the non-spatial analysis is used, while when the spatial analysis is used $CoV_{F_{max}}$ and $CoV_{D_{max}}$ are reduced by 85% and 33%, respectively, as presented in Table 3.

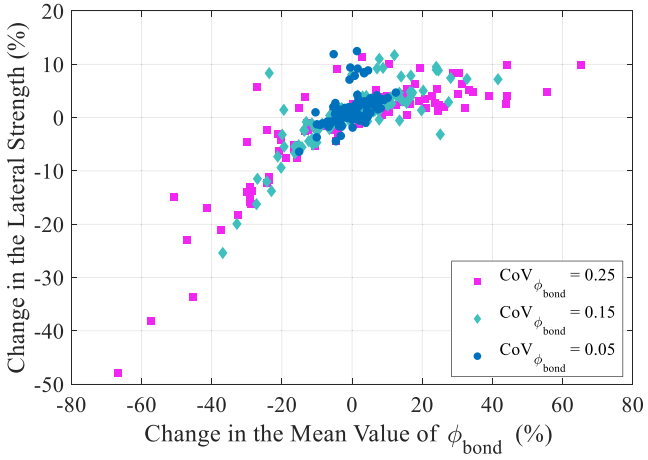

Fig. 9. Influence of the joint friction angle on the lateral force capacity of the wall in non-spatial stochastic analyses.

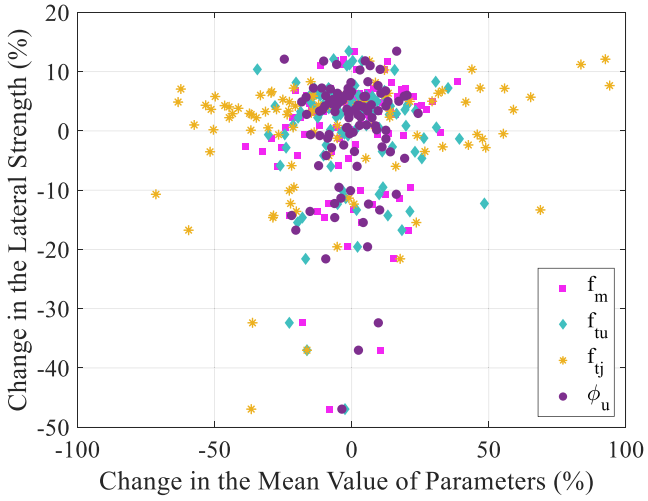

Fig. 10. Influence of the random parameters on the lateral force capacity of the wall in non-spatial stochastic analysis (benchmark case).

Fig. 9 helps to better understand the relationship between the joint friction angle and the lateral wall strength. A strong correlation is observed in all three coefficient of variations defined for the friction angle. Also, it is noted that the data points clustering becomes tighter as the $CoV_{\phi_{bond}}$ decreases. Additionally, the comparison between deterministic analyses (including the maximum (mean + standard deviation) and minimum (mean – standard deviation) values of joint friction angle) and non-spatial and spatial analyses are provided in the Appendix for the readers' reference.

Notice that the random parameters other than the joint friction angle

do not directly influence the wall's lateral strength within the predefined range of values and boundary conditions. Fig. 10 displays, for the benchmark case, how the strength of the wall changes according to the changes in the masonry compressive strength, unit and joint tensile strength, and the unit friction angle. This also demonstrates that no direct correlation of these parameters with the lateral strength can be inferred. Nonetheless, higher values of joint tensile strength will provide some correlation with the capacity, which can be forecasted from the top right quartile in Fig. 10.

5. Spatial correlation of modeling parameters

In statistical terms, correlation indicates the strength of the linear association between two random variables [57]. As stated, the construction process of masonry walls includes features that make one intuitively assume that some degree of spatial correlation should exist between the mechanical parameters of masonry. These features include but are not limited to the repetitive use of a single type of mortar and unit for most masonry types, a single mason constructing a specific part of the wall which implies uniform quality, same environmental conditions in the construction of a particular portion of the wall, and using the same batch of mortar for at least a specific length of the masonry course (s). However, very little effort was made on investigating the unit-to-unit or joint-to-joint correlation of the mechanical parameters of masonry. Stewart and Lawrence [58] showed that the strength and structural reliability of the wall is sensitive to flexural bond strength. Following that, Heffler et al. [24] conducted extensive laboratory work to determine the correlation of flexural bond strength. In their study, they carried out a bond wrench test for six full-sized clay brick masonry walls and used statistical analysis. Even though counter-intuitive, they concluded that a statistically significant correlation between adjacent unit flexural bond strengths does not exist. This finding is likely specific to the type of the wall studied (with a particular mortar and unit composition) and the types of structural analyses conducted. Furthermore, other parameters than the flexural bond strength should also be investigated. Indeed, Müller et al. [19] showed via numerical simulations that the degree of spatial correlation is important for single layer masonry walls under compression loading. Evidently, more experimental work should be conducted to determine whether a statistically significant correlation exists between the units and joints. Meanwhile, the effects of such a correlation are examined here via a stochastic discontinuum analysis.

5.1. Method of establishing the degree of spatial correlation

First, a methodology is established to investigate the effect of the spatial correlation of modeling parameters. It is noted that only the joint parameters are correlated, whereas no correlation is considered between the units. Also, the correlation is specified only for bed joints, while the head joints are not correlated. This assumption has a physical basis and is also confirmed by experimental testing [59]. The level of compressive stress and mortar compaction at a given point in the wall is different for head and bed joints, even though the materials used are theoretically the same. The differences in unit texture and the size effect of the areas of head and bed joints may lead to further deviation of mechanical properties. In addition, no correlation between the masonry courses of the wall is taken into account, based on the test results presented in [24]. Therefore, each course of the masonry wall is considered as a series of units and joints, where the parameters of the bed joints are correlated, and the head joints and units are not. In other words, both the unit and joint parameters have spatially varying properties. While there is spatial correlation within each course only for the joint parameters, each unit is assigned a different parameter value related to the units, *i.e.,* unit tensile strength and unit friction angle, for each realization of the 100 simulations.

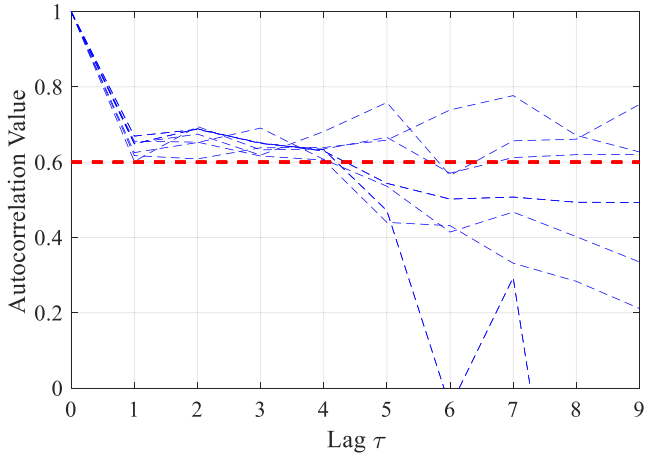

Fig. 11. A correlogram showing the autocorrelation values versus the lag.

In all spatial S-DA, the same spatially varying strength parameters are used for the units, *i.e.*, the same spatially varying unit properties are used in all the six cases investigated in this section of the study. On the other hand, the joint parameters (tensile strength and friction angle, and the compressive strength of masonry) are sampled in a way that the bed joints in the same course have designated values with the specified correlation while the head joints have uncorrelated random values. Note that the spatial correlation mentioned in this section is different from the correlation between the random variables in Table 2. The random variables sampled using the LHS method are statistically independent, as mentioned earlier. This is based on the information that there is no evidence of a physical connection between the random parameters considered in this study. Dependent variables represent the parameters with a physical relationship. The correlation of parameters evaluated here comprises only the spatial correlation of each joint parameter within each course of the masonry wall.

Following the description above, *i.e.*, considering the bed joints as a series of equispaced data points in space, the autocorrelation function is chosen as the mathematical tool to define a spatial correlation between the joints. The autocorrelation function, ρ_τ, presented in Equation (8), is a pair-wise calculation that is conducted for all pairs of values with a specific lag τ in the given data series, x_t.

$$\rho_\tau = \frac{\frac{1}{N}\sum_{i=1}^{N-\tau}(x_i-\bar{x})(x_{i+\tau}-\bar{x})}{\frac{1}{N}\sqrt{\sum_{i=1}^{N-\tau}(x_i-\bar{x})^2\sum_{i=1}^{N-\tau}(x_{i+\tau}-\bar{x})^2}}, \tau = 0,1,2,3,\cdots,(N-1) \quad (8)$$

where lag τ designates the number of units between the points in the series, N is the number of data points ($N = 10$ for each masonry course, see Fig. 6a), and $\bar{x}$ is the mean of the data series.

A caveat concerning the autocorrelation function presented in Equation (8) is that the "sample autocorrelation" conforms to the statistical literature and conflicts with the "lag τ sample autocorrelation" of the engineering literature that is widely used in signal processing. The autocorrelation function used in this study has a similar pattern to Pearson's product-moment correlation coefficient, which measures the strength of a linear association between two sets of data [57]. Therefore, one can infer from Equation (8) that ρ_τ measures the degree of correlation between each data point in the series and the point located τ units away from it. As expected, the autocorrelation function takes values between + 1 and –1. A value of + 1 indicates a perfect correlation between each value in the data series with the values τ units away from it. Similarly, a value of –1 indicates a perfectly negative correlation. If the value of the autocorrelation function is $\rho = 0$, then the values are statistically independent, and there is no correlation between the value of each joint in the masonry course and the joints τ units away from it. Finally, it should also be stated that there are various estimates of the autocorrelation function [60], but the one used in this study complies

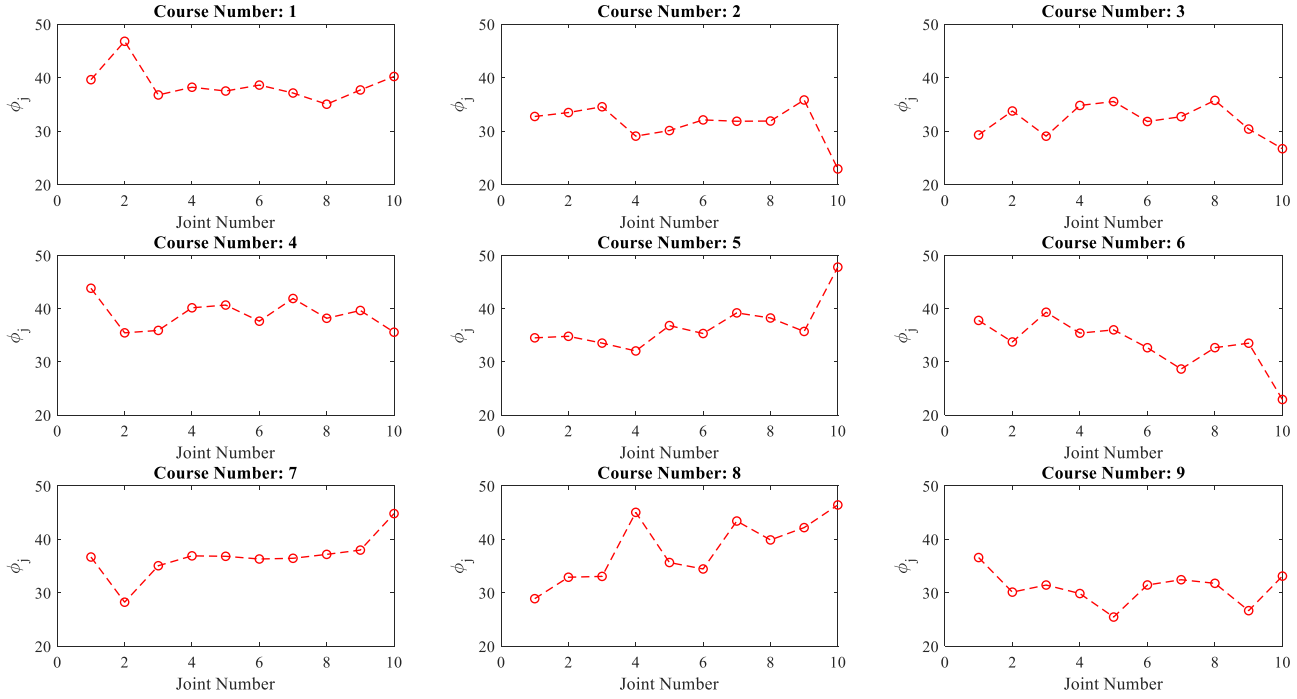

Fig. 12. An example figure displaying the value of joint friction angle for each joint in each masonry course.

Table 4
Average maximum force and displacement obtained from correlated spatial S-DA.

		$\rho = 0.65$ $CoV_{\phi_{bond}}$			$\rho = 0.85$ $CoV_{\phi_{bond}}$		
		0.25	**0.15**	**0.05**	**0.25**	**0.15**	**0.05**
F_{max} (kN)	Mean	120.44	128.25	130.50	119.06	128.51	130.55
	CoV	0.07	0.04	0.02	0.07	0.04	0.02
D_{max} (mm)	Mean	26.28	19.42	18.93	26.14	20.76	18.62
	CoV	0.28	0.36	0.30	0.31	0.35	0.30
# of sliding failure		64	15	3	66	20	4

with the work of Heffler et al. [24] and others to enable a direct comparison.

During the sampling of the correlated parameter values, N is taken as 10 since each wall course has ten joints. The mean values of the parameters given in Table 2 are used as $\bar{x}$. Based on the suggestions of Priestley [60] and Heffler et al. [24], the autocorrelation function values that fall within a band of $\pm 2\sqrt{1/N}$ (*i.e.*, approximately 0.60) are regarded as statistically not different from the case of no correlation, $\rho = 0$. Therefore, two cases of spatial correlation, one weak ($\rho = 0.65$) and one stronger ($\rho = 0.85$), are considered in this study in addition to the two cases taken into account earlier, *i.e.*, no correlation ($\rho = 0$) and full correlation ($\rho = 1$). In these two intermediary stages where $\rho = 0.65$ and $\rho = 0.85$, the parameter values sampled using the LHS were assigned an autocorrelation value sufficiently close to ρ for a lag of at least $\tau = 4$, meaning the joint parameter values are statistically correlated for a minimum four adjacent joints. This adjustment is shown in Fig. 11 as a correlogram where the autocorrelation values for the masonry compressive strength in each course of joints are plotted against the lag τ. The example belongs to simulation number 32, and the value of spatial correlation is $\rho = 0.65$. As can be observed, the ρ_τ value does not fall below the upper bound specified by $\pm 2\sqrt{1/N}$ for at least $\tau = 4$, and there is no further constraint on lag τ afterwards.

Fig. 12 illustrates how the joint friction angle values in each course vary in an example simulation. This example belongs to the case where $\rho = 0.65$ and the coefficient of variation for the friction angle is 0.15.

5.2. Results

As we investigate the results of the stochastic analyses, given in Table 3 and Table 4 together, the first striking observation is the decrease in the strength of the walls when $CoV_{\phi_{bond}} = 0.25$. The reason for this decline is premature sliding failures preventing the wall from reaching its full capacity. Indeed, when the number of sliding failures is investigated, it appears to be significantly high (64 and 66 for $\rho = 0.65$ and $\rho = 0.85$, respectively) compared to non-spatial ($\rho = 1$) and uncorrelated spatial ($\rho = 0$) cases. When the variation in the joint friction angle is reduced, the number of sliding failures also decreases, and the average of the maximum force attained increases. This phenomenon is also related to the fact that there is the highest probability of weak joints being surrounded by higher strength joints in the uncorrelated spatial case. Such distribution, *i.e.*, weak joint surrounded by strong ones, provides load redistribution once the weak joint fails. That is why the highest mean lateral strength is attained in uncorrelated spatial analysis.

Regarding the variation of the maximum force and displacement, there is no conspicuous change between the correlated spatial analysis cases, all being similar to each other. In general, the maximum force and displacement variations are much lower for spatial stochastic analyses. If this outcome can be generalized for various wall typology, geometry, and boundary conditions, then it might imply significant consequences in predicting the response of walls and, perhaps, defining performance limits. For example, the ability to predict the maximum forces with such a high precision might lead the research community to adopt strength-based performance criteria for stone masonry walls rather than displacement-based ones. As the difference between the peak forces is subtle, there would not be a significant difference in the wall's probability of failure if a strength-based reliability assessment is conducted.

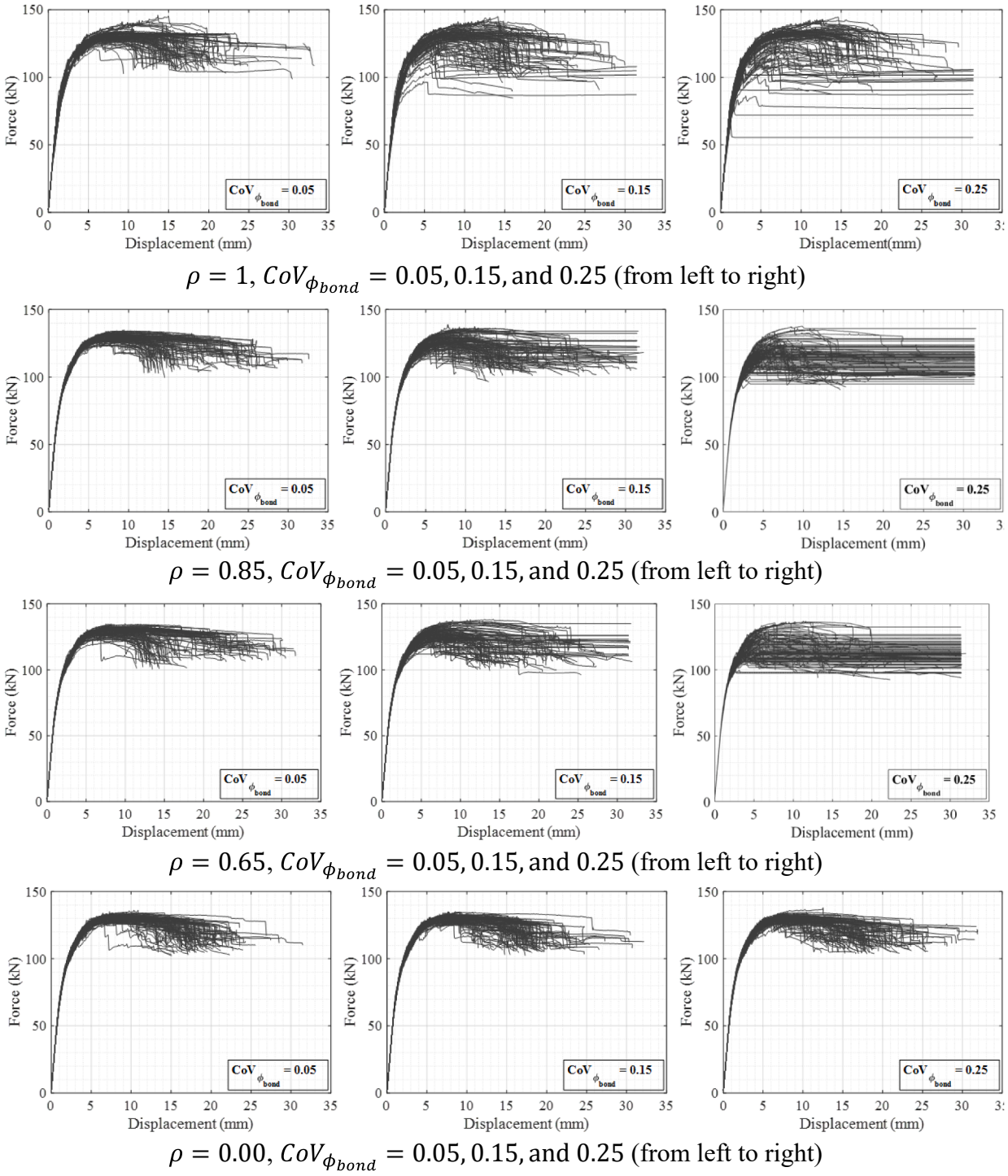

Fig. 13. Force-displacement graphs of all cases corresponding to various spatial correlation (ρ) and coefficient of variation of the joint friction angle ($CoV_{\phi_{bond}}$).

Also, for strength-based performance criteria, predicting the wall strength with higher precision may lead to calibration of the capacity modification factors for linear procedures.

The overall results of the analyses (1200 force–displacement curves in total) are presented in Fig. 13. The outcomes of this comprehensive analysis reveal the influence of the CoV of the friction angle on the macro response of the URM wall. It is worth noting that the obtained results are in line with the findings discussed by Li et al. [17] that the coefficient of variation of a modeling parameter, which has a direct effect on the strength, changes the CoV of the predicted strength values, and the spatial stochastic analysis significantly reduces the variation in the predicted strength values. In addition, the variations in the ultimate displacements decrease in non-spatial ($\rho = 1$) and uncorrelated spatial ($\rho = 0$) cases. Fig. 14 displays the histograms of the maximum force obtained from the uncorrelated spatial and non-spatial analyses. It illustrates the differences between the CoVs as the histograms of the

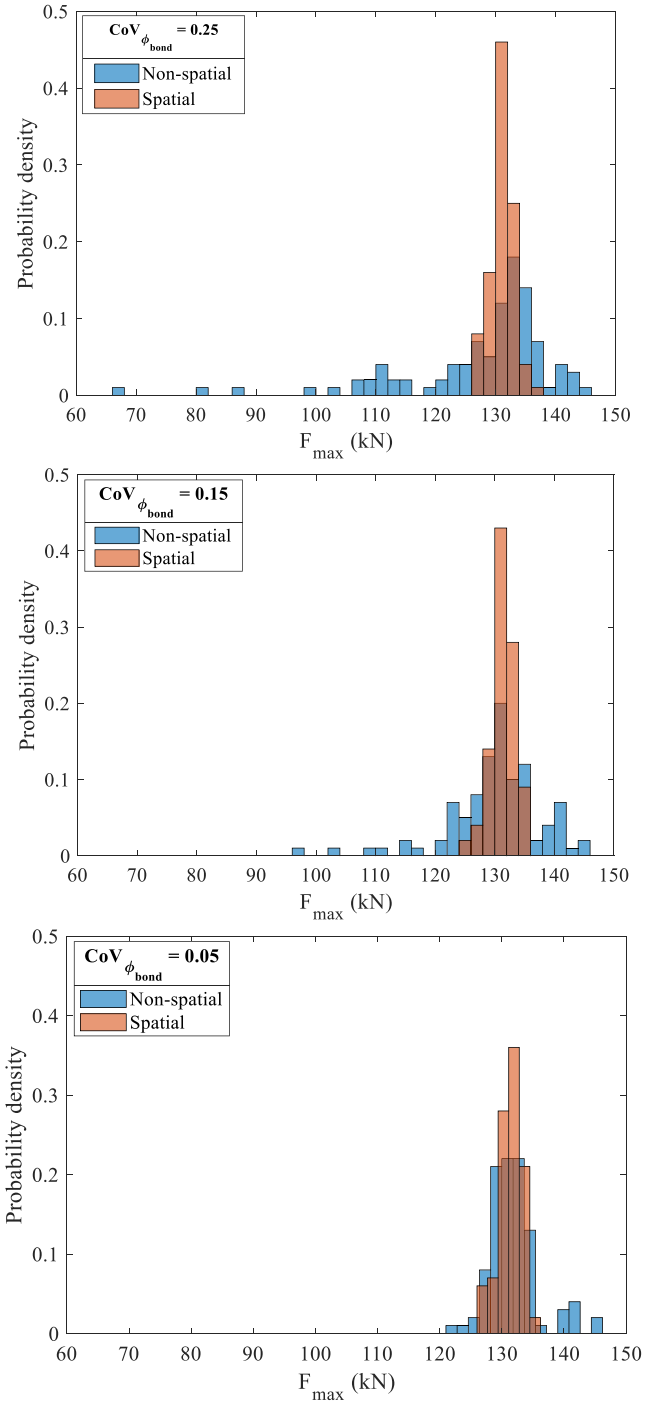

Fig. 14. Histograms of maximum lateral forces obtained in stochastic non-spatial and spatial analyses: $CoV_{\phi_{bond}}$= 0.25, 0.15, and 0.05 (from top to bottom).

spatial analyses are thinner and less dispersed. Also, notice that the dispersion in non-spatial analyses diminishes as the $CoV_{\phi_{bond}}$ reduces, and becomes very close to the spatial case in Fig. 14c.

6. Conclusions

The present study investigates the effect of material uncertainty on the in-plane behavior and capacity of stone URM walls subjected to lateral loading, using a stochastic discontinuum analysis framework. The outcomes of this research can be summarized as follows.

The results demonstrate the significant differences between the results of spatial and non-spatial stochastic discontinuum analyses. They emphasize the significance of considering the spatial variation of parameters in analyzing URM walls. It is observed that by considering unit-to-unit and joint-to-joint spatial variability of the masonry properties, the damage progression and failure mechanisms captured in the numerical models are closer to the experimental finding. Accordingly, the results suggest that considering spatial variability of modeling parameters significantly decreases the variation in the force and displacement capacities and leads to a more reliable prediction of the behavior. Note that reducing the CoV of the lateral strength and ultimate displacement may also necessitate fewer simulations when the MCS is employed.

In the presence of joint-to-joint correlation of modeling parameters, the results indicate: *i*) as the correlation increases, the results resemble the non-spatial analysis results, *ii*) if the CoV of friction angle is high, premature sliding failures can occur that may not be physically sensible. In other words, the simplified micro-modeling may suggest sliding failure, particularly true for the cases where $0.65 \leq \rho \leq 0.85$ and $CoV_{\phi_{bond}} \geq 0.10$, which is less likely to be observed physically in reality. Therefore, considering the joint-to-joint correlation in the spatial analysis may not be necessary.

Except for one parameter (joint friction angle), no direct relationship between the wall's lateral strength and the random parameters could be observed. A strong correlation between the joint friction angle and the wall's in-plane strength is found. Moreover, the uncertainty in the joint friction angle value and its effect on the results are quantified. The influence of the initial assumptions on the obtained results should be acknowledged. As the bond friction angle value and its coefficient of variation are not easy to obtain experimentally, one should be careful about the initial assumptions of distribution parameters, especially when conducting non-spatial stochastic analysis. Conversely, the influence of $CoV_{\phi_{bond}}$ on the results is found minimal in spatial S-DA; hence, highlighting an appealing feature of spatial S-DA in case of lack of data.

Even though the proposed stochastic discontinuum analysis methodology can reliably predict the strength of the masonry walls, its greater purposes are quantifying the uncertainty in strength and displacement prediction and determining the performance criteria for masonry walls. It requires various types of walls with different geometry, boundary conditions, and input parameters to be considered. With the aid of improved stochastic models, performance criteria for various loading conditions can be determined, and systematic reliability analyses can be performed so that the safety for masonry walls provided in the codes and standards is adequately verified.

The current work will be extended to URM walls with different aspect ratios, construction types, and boundary conditions in the future study. Further analyses are also required to assess the out-of-plane behavior of URM walls, including the material uncertainties.

CRediT authorship contribution statement

Semih Gonen: Conceptualization, Methodology, Software, Validation, Formal analysis, Visualization, Writing – original draft, Writing – review & editing. **Bora Pulatsu:** Conceptualization, Methodology, Software, Validation, Formal analysis, Visualization, Writing – original draft, Writing – review & editing. **Ece Erdogmus:** Writing – review & editing. **Paulo B. Lourenço:** Writing – review & editing. **Serdar Soyoz:** Writing – review & editing.

Declaration of Competing Interest

The authors declare that they have no known competing financial interests or personal relationships that could have appeared to influence the work reported in this paper.

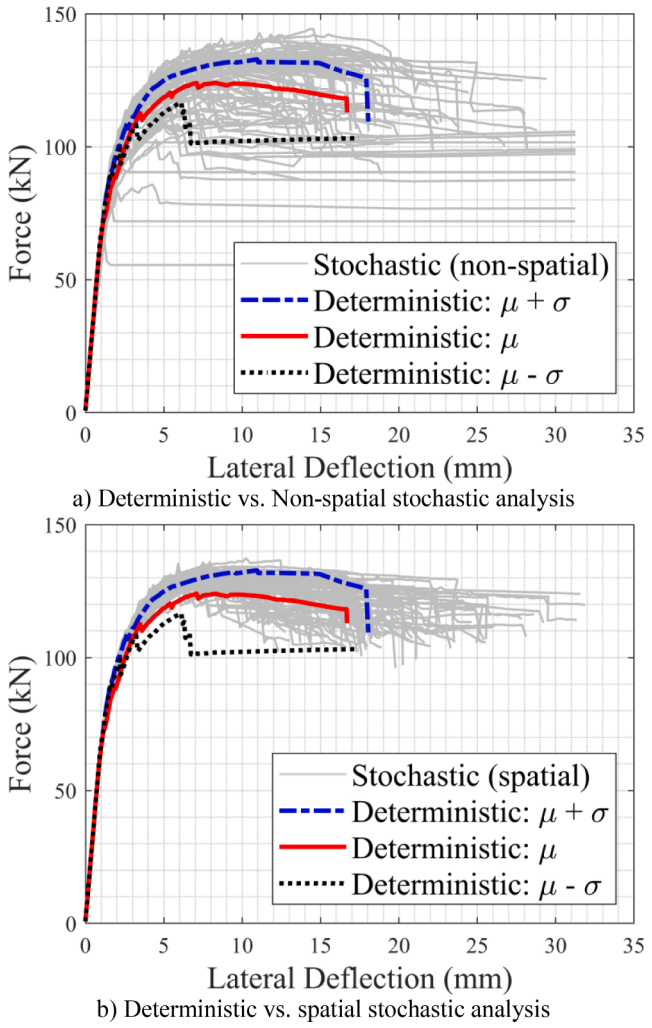

Fig. 15. Results of the spatial and non-spatial analyses for $CoV_{\phi_{bond}} = 0.25$ are compared to the deterministic analysis results.

Appendix

Fig. 15.

References

[1] G. Vlachakis, E. Vlachaki, P.B. Lourenço, Learning from failure: Damage and failure of masonry structures, after the 2017 Lesvos earthquake (Greece), Eng Fail Anal 117 (2020), 104803, https://doi.org/10.1016/j.engfailanal.2020.104803.

[2] S. Akkar, A. Aldemir, A. Askan, S. Bakir, E. Canbay, I.O. Demirel, et al., 8 March 2010 elaziğ-kovancilar (Turkey) Earthquake: Observations on ground motions and building damage, Seismol Res Lett 82 (2011) 42–58, https://doi.org/10.1785/gssrl.82.1.42.

[3] A. Shabani, M. Kioumarsi, M. Zucconi, State of the art of simplified analytical methods for seismic vulnerability assessment of unreinforced masonry buildings, Eng Struct 239 (2021), 112280, https://doi.org/10.1016/j.engstruct.2021.112280.

[4] J. Park, P. Towashiraporn, J.I. Craig, B.J. Goodno, Seismic fragility analysis of low-rise unreinforced masonry structures, Eng Struct 31 (2009) 125–137, https://doi.org/10.1016/j.engstruct.2008.07.021.

[5] S. Gonen, S. Soyoz, Reliability-based seismic performance of masonry arch bridges, Struct Infrastruct Eng (2021) 1–16, https://doi.org/10.1080/15732479.2021.1918726.

[6] B. Pulatsu, S. Gonen, E. Erdogmus, P.B. Lourenço, J.V. Lemos, J. Hazzard, Tensile Fracture Mechanism of Masonry Wallettes Parallel to Bed Joints: A Stochastic Discontinuum Analysis, Model Open Access J Model Eng Sci 1 (2020) 78–93, https://doi.org/10.3390/modelling1020006.

[7] V. Bosiljkov, D. D'Ayala, V. Novelli, Evaluation of uncertainties in determining the seismic vulnerability of historic masonry buildings in Slovenia: use of macro-element and structural element modelling, Bull Earthq Eng 13 (2015) 311–329, https://doi.org/10.1007/s10518-014-9652-7.

[8] A.C. Isfeld, E. Moradabadi, D.F. Laefer, N.G. Shrive, Uncertainty analysis of the effect of grout injection on the deformation of multi-wythe stone masonry walls, Constr Build Mater 126 (2016) 661–672, https://doi.org/10.1016/j.conbuildmat.2016.09.058.

[9] M. Tondelli, M. Rota, A. Penna, G. Magenes, Evaluation of uncertainties in the seismic assessment of existing masonry buildings, J Earthq Eng 16 (2012) 36–64, https://doi.org/10.1080/13632469.2012.670578.

[10] H. Derakhshan, K.Q. Walsh, J.M. Ingham, M.C. Griffith, D.P. Thambiratnam, Seismic fragility assessment of nonstructural components in unreinforced clay brick masonry buildings, Earthq Eng Struct Dyn 49 (2020) 285–300, https://doi.org/10.1002/eqe.3238.

[11] D. Malomo, M.J. DeJong, A. Penna, Influence of Bond Pattern on the in-plane Behavior of URM Piers, Int J Archit Herit 00 (2019) 1–20, https://doi.org/10.1080/15583058.2019.1702738.

[12] B. Pulatsu, E.M. Bretas, P.B. Lourenço, Discrete element modeling of masonry structures: Validation and application, Earthquakes Struct 11 (2016) 563–582, https://doi.org/10.12989/eas.2016.11.4.563.

[13] R.K. Napolitano, B. Glisic, Understanding the function of bonding courses in masonry construction: An investigation with mixed numerical methods, J Cult Herit 39 (2019) 120–129, https://doi.org/10.1016/j.culher.2019.03.007.

[14] B. Pulatsu, F. Gencer, E. Erdogmus, Study of the effect of construction techniques on the seismic capacity of ancient dry-joint masonry towers through DEM, Eur J Environ Civ Eng (2020) 1–18, https://doi.org/10.1080/19648189.2020.1824823.

[15] S. Gonen, S. Soyoz, Investigations on the elasticity modulus of stone masonry, Structures 30 (2021) 378–389, https://doi.org/10.1016/j.istruc.2021.01.035.

[16] Semih Gonen, Reliability-based Seismic Assessment of Masonry Arch Bridges, Boğaziçi University, 2020.

[17] J. Li, M.J. Masia, M.G. Stewart, S.J. Lawrence, Spatial variability and stochastic strength prediction of unreinforced masonry walls in vertical bending, Eng Struct 59 (2014) 787–797, https://doi.org/10.1016/j.engstruct.2013.11.031.

[18] J. Li, M.J. Masia, M.G. Stewart, Stochastic spatial modelling of material properties and structural strength of unreinforced masonry in two-way bending, Struct Infrastruct Eng 13 (2017) 683–695, https://doi.org/10.1080/15732479.2016.1188125.

[19] D. Müller, V. Förster, C.-A. Graubner, Influence of material spatial variability on required safety factors for masonry walls in compression, Mauerwerk 21 (2017) 209–222, https://doi.org/10.1002/dama.201700004.

[20] L.J. Gooch, M.J. Masia, M.G. Stewart, Application of stochastic numerical analyses in the assessment of spatially variable unreinforced masonry walls subjected to in-plane shear loading, Eng Struct 235 (2021), 112095, https://doi.org/10.1016/j.engstruct.2021.112095.

[21] S. Gonen, B. Pulatsu, S. Soyoz, E. Erdogmus, Stochastic discontinuum analysis of unreinforced masonry walls: Lateral capacity and performance assessments, Eng Struct 238 (2021), 112175, https://doi.org/10.1016/j.engstruct.2021.112175.

[22] B. Pulatsu, S. Gonen, E. Erdogmus, P.B. Lourenço, J.V. Lemos, R. Prakash, In-plane structural performance of dry-joint stone masonry Walls: A spatial and non-spatial stochastic discontinuum analysis, Eng Struct 242 (2021), 112620, https://doi.org/10.1016/j.engstruct.2021.112620.

[23] V. Sarhosis, T. Forgacs, J.V. Lemos, Stochastic strength prediction of masonry structures: a methodological approach or a way forward? RILEM Tech Lett 4 (2020) 122–129, https://doi.org/10.21809/rilemtechlett.2019.100.

[24] L. Heffler, M.G. Stewart, M. Masia, M. Correa, Statistical Analysis and Spatial Correlation of Flexural Bond Strength for Masonry Walls, Mason Int 21 (2008) 59–70.

[25] J. Li, M.G. Stewart, M.J. Masia, S.J. Lawrence, Spatial Correlation of Material Properties and Structural Strength of Masonry in Horizontal Bending, J Struct Eng 142 (2016) 04016112, https://doi.org/10.1061/(asce)st.1943-541x.0001488.

[26] M. Tabbakhha, G. Deodatis, Effect of Uncertainty of Tensile Strength of Mortar Joints on the Behavior of Masonry Walls under Lateral Loads, J Struct Eng 143 (2017) 04016166, https://doi.org/10.1061/(asce)st.1943-541x.0001640.

[27] A.C. Isfeld, M.G. Stewart, M.J. Masia, Stochastic finite element model assessing length effect for unreinforced masonry walls subjected to one-way vertical bending under out-of-plane loading, Eng Struct 236 (2021), 112115, https://doi.org/10.1016/j.engstruct.2021.112115.

[28] M.A. Erberik, Generation of fragility curves for Turkish masonry buildings considering in-plane failure modes, Earthq Eng Struct Dyn 37 (2008) 387–405, https://doi.org/10.1002/eqe.760.

[29] M. Rota, A. Penna, G. Magenes, A methodology for deriving analytical fragility curves for masonry buildings based on stochastic nonlinear analyses, Eng Struct 32 (2010) 1312–1323, https://doi.org/10.1016/j.engstruct.2010.01.009.

[30] S. Gonen, B. Pulatsu, E. Erdogmus, E. Karaesmen, E. Karaesmen, Quasi-Static Nonlinear Seismic Assessment of a Fourth Century A.D. Roman Aqueduct in Istanbul, Turkey, Heritage 4 (2021) 401–421, https://doi.org/10.3390/heritage4010025.

[31] E. Vanmarcke, M. Shinozuka, S. Nakagiri, G.I. Schuëller, M. Grigoriu, Random fields and stochastic finite elements, Struct Saf 3 (1986) 143–166, https://doi.org/10.1016/0167-4730(86)90002-0.

[32] F. Parisi, N. Augenti, Uncertainty in seismic capacity of masonry buildings, Buildings 2 (2012) 218–230, https://doi.org/10.3390/buildings2030218.

[33] S. Saloustros, L. Pelà, F.R. Contrafatto, P. Roca, I. Petromichelakis, Analytical Derivation of Seismic Fragility Curves for Historical Masonry Structures Based on Stochastic Analysis of Uncertain Material Parameters, Int J Archit Herit 13 (2019) 1142–1164, https://doi.org/10.1080/15583058.2019.1638992.

[34] S. Saloustros, L. Pelà, P. Roca, Nonlinear Numerical Modeling of Complex Masonry Heritage Structures Considering History-Related Phenomena in Staged Construction Analysis and Material Uncertainty in Seismic Assessment, J Perform

Constr Facil 34 (2020) 04020096, https://doi.org/10.1061/(asce)cf.1943-5509.0001494.
[35] P. Roca, M. Cervera, G. Gariup, L. Pela, Structural analysis of masonry historical constructions. Classical and advanced approaches, Arch Comput Methods Eng 17 (2010) 299–325, https://doi.org/10.1007/s11831-010-9046-1.
[36] F. Parisse, S. Cattari, R. Marques, P.B. Lourenço, G. Magenes, K. Beyer, B. Calderoni, G. Camata, E.A. Cordasco, M.A. Erberik, C. İçel, M. Karakaya, D. Malomo, C.F. Manzini, C. Marano, F. Messali, G. Occhipinti, B. Pantò, Ö. Saygılı, M. Sousamli, Benchmarking the seismic assessment of unreinforced masonry buildings from a blind prediction test, Structures 31 (2021) 982–1005.
[37] D. Malomo, M.J. DeJong, A. Penna, Distinct element modelling of the in-plane cyclic response of URM walls subjected to shear-compression, Earthq Eng Struct Dyn 48 (2019) 1322–1344, https://doi.org/10.1002/eqe.3178.
[38] C. Chácara, F. Cannizzaro, B. Pantò, I. Caliò, P.B. Lourenço, Seismic vulnerability of URM structures based on a Discrete Macro-Element Modeling (DMEM) approach, Eng Struct 201 (2019), 109715, https://doi.org/10.1016/j.engstruct.2019.109715.
[39] I. Caliò, M. Marletta, B. Pantò, A new discrete element model for the evaluation of the seismic behaviour of unreinforced masonry buildings, Eng Struct 40 (2012) 327–338, https://doi.org/10.1016/j.engstruct.2012.02.039.
[40] S. Saloustros, L. Pelà, P. Roca, J. Portal, Numerical analysis of structural damage in the church of the Poblet Monastery, Eng Fail Anal 48 (2015) 41–61, https://doi.org/10.1016/j.engfailanal.2014.10.015.
[41] Cundall PA. A computer model for simulating progressive, large-scale movements in blocky rock systems. Int. Symp. Rock Mech., vol. 2, Nancy: 1971, p. 47–65.
[42] M. Godio, I. Stefanou, K. Sab, Effects of the dilatancy of joints and of the size of the building blocks on the mechanical behavior of masonry structures, Meccanica 53 (2018) 1629–1643, https://doi.org/10.1007/s11012-017-0688-z.
[43] B. Pulatsu, E. Erdogmus, P.B. Lourenço, J.V. Lemos, K. Tuncay, Simulation of the in-plane structural behavior of unreinforced masonry walls and buildings using DEM, Structures 27 (2020) 2274–2287, https://doi.org/10.1016/j.istruc.2020.08.026.
[44] B. Pulatsu, S. Kim, E. Erdogmus, P.B. Lourenço, Advanced analysis of masonry retaining walls using mixed discrete-continuum approach, Proc Inst Civ Eng - Geotech Eng 174 (3) (2021) 302–314.
[45] J.C. Quezada, E. Vincens, R. Mouterde, J.C. Morel, 3D failure of a scale-down dry stone retaining wall: A DEM modelling, Eng Struct 117 (2016) 506–517, https://doi.org/10.1016/j.engstruct.2016.03.020.
[46] P.A. Cundall, C. Detournay, Dynamic relaxation applied to continuum and discontinuum numerical models in geomechanics, CRC Press, Rock Mech. Eng., 2017, pp. 57–102.
[47] B. Pulatsu, E. Erdogmus, P.B. Lourenço, J.V. Lemos, J. Hazzard, Discontinuum analysis of the fracture mechanism in masonry prisms and wallettes via discrete element method, Meccanica 55 (2020) 505–523, https://doi.org/10.1007/s11012-020-01133-1.
[48] B. Pulatsu, E. Erdogmus, P.B. Lourenço, R. Quey, Simulation of uniaxial tensile behavior of quasi-brittle materials using softening contact models in DEM, Int J Fract 217 (2019) 105–125, https://doi.org/10.1007/s10704-019-00373-x.
[49] E. Erdogmus, B. Pulatsu, A. Gaggioli, M. Hoff, Reverse Engineering a Fully Collapsed Ancient Roman Temple through Geoarchaeology and DEM, Int J Archit Herit 00 (2020) 1–21, https://doi.org/10.1080/15583058.2020.1728593.
[50] E. Çaktı, Ö. Saygılı, J.V. Lemos, C.S. Oliveira, Discrete element modeling of a scaled masonry structure and its validation, Eng Struct 126 (2016) 224–236, https://doi.org/10.1016/j.engstruct.2016.07.044.
[51] Ö. Saygılı, J.V. Lemos, Investigation of the Structural Dynamic Behavior of the Frontinus Gate, Appl Sci 10 (2020) 5821, https://doi.org/10.3390/app10175821.
[52] J.V. Lemos, Contact representation in rigid block models of masonry, Int J Mason Res Innov 2 (2017) 321, https://doi.org/10.1504/ijmri.2017.10008298.
[53] Itasca Consulting Group Inc. 3DEC Three Dimensional Distinct Element Code 2013.
[54] Lourenço PB. Recent advances in masonry structures: Micromodelling and homogenisation, in: Multiscale Modeling in Solid Mechanics: Computational Approaches. Multiscale Model. solid Mech. Comput. approaches, 2009, p. 251–94.
[55] M. Stein, Large sample properties of simulations using latin hypercube sampling, Technometrics 29 (1987) 143–151, https://doi.org/10.1080/00401706.1987.10488205.
[56] A. Olsson, G. Sandberg, O. Dahlblom, On Latin hypercube sampling for structural reliability analysis, Struct Saf 25 (2003) 47–68, https://doi.org/10.1016/S0167-4730(02)00039-5.
[57] Percival DB, Walden AT. Spectral Analysis for Univariate Time Series. Cambridge University Press; 2020. doi:10.1017/9781139235723.
[58] M.G. Stewart, S. Lawrence, Structural reliability of masonry walls in flexure, Mason Int 15 (2) (2002) 48–52.
[59] Masia MJ, Simundic G, Page AW. The flexural strength of stack bonded masonry stage 1 – A preliminary study. Proc. 9th Int. Mason. Conf., Guimarães, Portugal: 2014.
[60] Priestley MB. Spectral Analysis and Time Series Volume I - Univariate Series. London, UK: Academic Press; 1981.